Hochschule Bremen
Neustadtswall 30, 28199 Bremen
Fakultät 5 - Natur und Technik
IS Bionik B. Sc. 7. Semester

HSB
Hochschule Bremen
City University of Applied Sciences

Biomimetic lightweight optimization for compression-loaded structures inspired by the cocoon of *Hirudo sp.*

Bachelorthesis

Modul 7.1 Bachelor

Author: Tino Marte, Nr. 5259915
Supervisors: Prof. Dr. J.-H. Dirks, Prof. Dr.-Ing. J. Muessig

Timeframe: 09. October 2025 - 11. December 2025

Acknowledgements

My utmost gratitude to the army of great people that have made it possible for me to get to this point. Both my supervisors, Prof. Dr. Dirks and Prof. Dr.-Ing Muessig, provided extensive resources and input to this work and helped improve it uncountable times. The high opinions I already held of them were surpassed tenfold.

A massive thanks to my parents and the rest of my family who have assisted me on this journey, such as my grandma and my brother. Their extensive support in every imaginable way has made it possible for me to fully dedicate myself to my studies, on top of helping with proof reading.
All the best wishes to my colleagues in Thessaloniki, Savvas, Thomas, Manolis, Giannis and Prof. Tzetzis, who taught me the tools necessary for large portions of the methodology used in this thesis. Thank you to everyone who has directly and indirectly supported me through the trials and tribulations that this undergraduate program throws your way, so that I could even get this far. Names like Dr. Graupner, René Sonntag and Florian Huber come to mind, aside from my fellow peers Daniel and Saad. Especially Dr. Graupner who was also an invaluable asset with her extensive experience in material testing, on top of the kindness and respect she shows to all students. Another thanks to Dr. Stefan Kammer of Animalpharma for providing the Cocoons and PD Dr. Christian Müller for introducing the research topic to my supervisor, where it ended up with me. Thanks to all my fellow Bachelor and PHD candidates who took part at the meetings, where the recent developments of our research were discussed. Even those that are not mentioned here, a more indirect thank you to anyone who showed kindness towards me during this journey, helping me push through tough times like health scares or mental struggles. Another huge thank you to the creator and leader of the best undergraduate program ever, Prof. Dr. Kesel. This opportunity was only made available to me through her direct contributions and dedication to the field of biomimetics.
To close, the greatest, unimaginably huge and terrific thank you to my most valuable asset through all of my studies, life and this thesis in particular and also my best friend, Matteo. His contributions are too numerous to list in full, but for this thesis he worked overtime to produce high quality 3D-prints of compression specimens with highly intricate structures, which made a near insurmountable challenge solvable with a simple text message.

Abstract

The cocoons of *Hirudo sp.* are currently assumed to mainly serve as protection from desiccation. Their complex, cellular wall structure was examined and biomimetically translated into a lightweighting algorithm. Geometries created by this algorithm showed of up to 3.5 times higher resistance to radial buckling, when compared to uniform shells, despite consisting of less mass, in both finite element analysis and compression tests. This hints at a mechanical optimization of the cocoons, that inspired these structures, and opens the way for new research to verify this claim. A further optimization of the algorithm's gradients could make it possible to create structures with high mechanical performance in regards to radial buckling resistance.

Keywords: biomimetic design, leech cocoon, lightweighting, implicit modeling, Voronoi structures

Contents

List of Figures

List of Tables

1 Introduction

Many different species of the Hirudinae family produce cocoons with wall structures ranging from thin and membranous to thick and foam-like (Maitland et al., 2000; Phillips et al., 2020). Medicinal leeches, *Hirudo sp.*, lay their eggs into a foam that is secreted from the clitellum. The foam is then deposited in substrate, where it dries around the eggs into such a cocoon.
The cocoon's structure along with the mechanisms it provides for an evolutionary benefit have been subjects of minor attention in biology. Saidel et al. (2018) investigated the complex microstructure by using scanning electron microscopy (SEM). It consists of an inner closed wall surrounded by a network of thin beams that shows a radial gradient of thickness. This remarkable complexity is showcased in Figure 1a. The proposed purpose of this structure is as desiccation protection, since areas of high silicon content were found on the outer edges, which might be an indicator. But as noted by the authors, this was primarily the case in the areas in contact with the silicon-rich substrate, meaning integration could be a direct result of contamination, not an intentional mechanism. As other literature is scarce, the assumption can be made that the current accepted hypothesis is that the purpose of the complex wall structure is to specifically protect from desiccation. Despite this, the lack of support for this claim warrants skepticism.

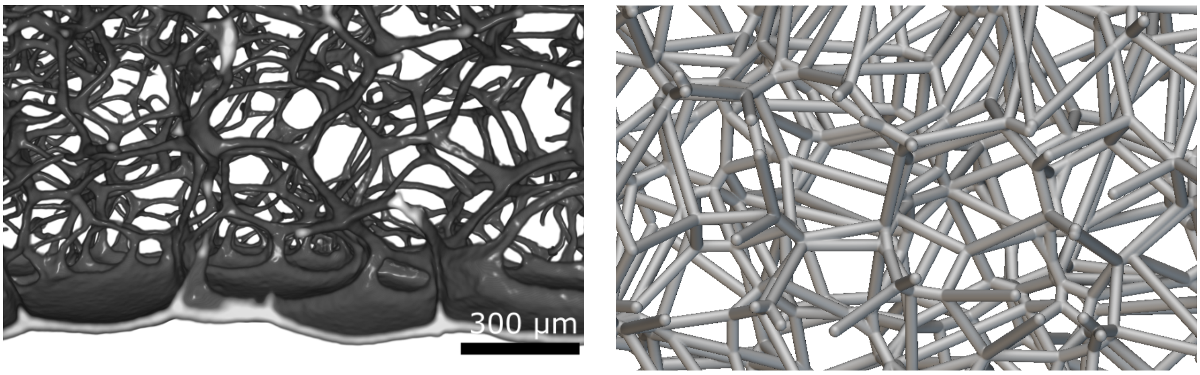

(a) (b)

Figure 1: Cocoon wall compared to an artificial Voronoi structure. In (a), a volume visualization of a section of the cocoon wall of *Hirudo sp.* is shown. Clearly visible is the fully closed inner wall at the bottom. Connected to it, the outer network of thin beams can be found. Depicted in (b) is an artificially generated Voronoi lattice. They both consist of stochastic cells, forming a network of thin interconnected beams.

The network of stochastic cells consisting of interconnected, thin beams found in the cocoon wall can be described as a three dimensional Voronoi lattice (s. Figure 1). Such lattices are created from randomly distributed points in space. The space is then divided into cells with the nearest neighbour rule, by projecting spheres outward from each point. Through the lines where two spheres intersect, the faces of the cells are created (Schliecker, 2002). This closely mimics the process that produced the solid cocoon, where otherwise spherical foam bubbles intersect with one another and form sharp edged intersections. The solidificaion of the foam only leaves solid material at the outer edges of these intersections, creating thin beams (Saidel et al., 2018). With the introduction off additive manufacturing, the creation of intentionally designed cellular materials has been made possible (Maiti et al., 2016; Yang et al., 2018). These technological advances have reignited interest in Voronoi structures, which are known for their energy absorp-

tion, isotropy and progressive collapse properties (Efstathiadis et al., 2023; Feng et al., 2023; Yuan et al., 2023).
With the new manufacturing possibilities, an advancement in design tools to take advantage of the opportunities was needed. Implicit modeling, that calculates volumes from spacial functions, is a new approach that overcomes the shortcomings of surface based modeling for additive manufacturing (Li et al., 2018). The commercial software named nTop (previously nTopology) is a novel, industry focused tool that makes the utilization of this technique easily approachable with its block based workflows. Its data structures show the potential to increase optimization efficiency of complex, volumetric geometries by three orders of magnitude through implicit modeling (Groen et al., 2021). This makes it possible to easily create algorithms that can produce organic, complex geometries.
The advent of these technologies is of particular interest to the field of biomimetics, as many different iterations of biomimetic cellular structures have found success in lightweighting applications (Hu et al., 2017). Biomimetics refers to the interdisciplinary approach of solving technological problems by getting inspiration from the solutions organisms have developed. This is accomplished by the abstraction, transfer and application of the knowledge gained from the bio-inspiration to the specific problem (Verein Deutscher Ingenieure, 2012).

All bio-material the leech uses to produce the cocoon cannot be expended on its own survival. Cellular structures can be optimized for different applications with the introduction of gradients (Hübner et al., 2023). Therefore, it is likely that the cocoon has been evolutionarily optimized to provide its function at the lowest mass possible.
Though the loads that a cocoon must endure while embedded in substrate have not been studied, it is assumed here that such loads would take the form of forces in the radial direction, which may lead to buckling. The radial buckling load (RBL) is a term referring to the critical compression force in the radial direction, at which a sudden instability of thin-walled structures, such as pipes, occurs (Li et al., 2011; Ou et al., 2023; Widiyanto et al., 2022). In these contexts, the load is applied evenly as pressure across the entire radius. It is assumed that the forces cocoons have to withstand may not be equally distributed. Therefore, radial buckling will refer to the buckling of thin-walled structures from an unevenly applied compression force in the scope of this thesis. Radial buckling could endanger the integrity of the eggs and present a major evolutionary pressure. The curved cocoon walls may have been evolutionarily optimized to increase the RBL as a response to this. If this is the case, these structures may be of interest for lightweighting applications.

The goal of this thesis is to investigate the currently accepted hypothesis that the cocoon's wall structure serves mainly as protection from desiccation, by analyzing lightweighting structures inspired by the leech cocoon for their mechanical performance. To evaluate if any optimizations are present, the natural point of comparison is an unoptimized uniform shell.
Such an investigation may not only lead to a novel lightweight structure, but also give insights into the evolutionary pressures that leeches are subjected to.
As a definition for its scope, a hypothesis is introduced that reflects the current understanding of the purpose of the cocoons.

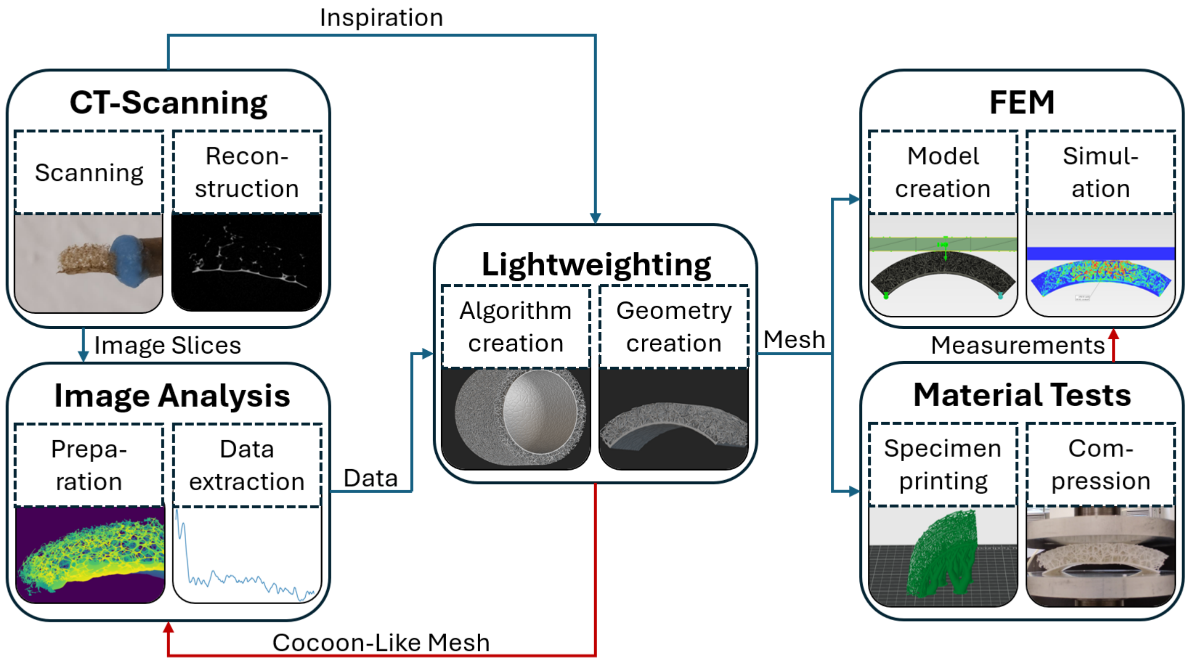

Figure 2: Methodology Chart. Results being transferred from one step to the next are represented by blue arrows. Validation dependencies are depicted as red arrows. Below each step, a visualization of the process is provided.

Hypothesis 1. *Applying a leech-cocoon-inspired lightweighting algorithm to a curved part does not lead to a higher radial buckling load than a uniform shell operation, that achieves the same mass reduction.*

Because the cocoon itself is curved, it is likely that its wall structure would be optimized for its specific geometry. For a lightweighting algorithm to be of use in a variety of technological applications, it has to be applicable to a variety of geometries. Edges may interact unfavourably with a lightweighting structure optimized for curves. Not being able to use edges would represent a major design constraint. For this reason a second Hypothesis is proposed that builds upon the first.

Hypothesis 2. *Hypothesis 1 is also true for a part with a sharp edge.*

2 Materials and Methods

To verify the hypotheses, cocoons will be analyzed, an algorithm will be created based on the findings that will be applied to curved and edged geometries, their RBL will be evaluated in a finite element analysis (FEA) and the results evaluated by performing compression tests on 3D-printed specimens. A methodology chart visualizing the process can be in Figure 2.

2.1 Cocoon Sourcing

Both dry and fresh cocoons of *Hirudo sp.* were sourced from Animalpharma (Ketzin, Germany). While the dried cocoons were already cut open and kept inside of a plastic jar, the fresh cocoons were instead received embedded in wet substrate (pH = 6.6) before the leeches had hatched. Then the cocoons were kept inside the substrate and monitored. Every time leeches had hatched,

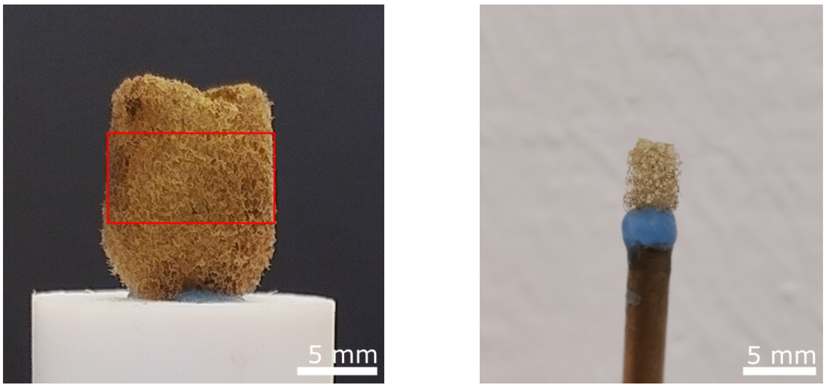

(a) (b)

Figure 3: Specimen preparation. Depicted in (a) is a cocoon specimen that is attached to a piece of polymer with blue adhesive wax. The area, where the wall section specimens were taken from, is marked by a red rectangle. In (b), a wall section specimen is shown. It is attached to a rod shaped implement with the same adhesive wax as the cocoon specimen.

they were extracted from the substrate and euthanized in a solution of 15 % ethanol. After all activity had subsided inside the cocoons, they were transferred to air tight plastic tubes for a few days until inspection.

2.2 Computed Tomography (CT)-Scanning

The cocoon's three dimensional structure was examined with a Micro-CT-Scanner (Skyscan 1275, Bruker, Billerica, Massachusetts, USA). All scans were performed with the X-ray source settings of 40 kV and 60 µA. One full cocoon of each type was scanned with a pixel size of 18 µm. They were attached upright to a cylindrical piece of polymer with adhesive wax, which was itself attached to a circular sample plate implement the same way (s. Figure 3a).
Also, ten rectangular specimens with side lengths varying from 4 to 6 mm were prepared by cutting them out of the walls of dry cocoons with a scalpel. They were extracted at similar positions in the middle of the long sides of the cocoons, where the curvature is the lowest. The attachment to the tip of a rod shaped implement was also performed with adhesive wax (s. Figure 3b). Scans of these specimens used a pixel size of 7.08 µm and will be further examined in the image analysis. No rectangular samples from fresh cocoons were analyzed, due to the quick shrinking from loss of moisture leading to unreliable results. After scanning, the raw image output was reconstructed into image slices using NRecon (Version: 2.2.0.6, Bruker, Billerica, Massachusetts, USA). Here, a single step of post-alignment fine tuning was performed with 5 trials and a parameter step of 1.0. The collective of all image slices reconstructed from the scans of one specimen will be referred to as a scan in further processing steps.

2.3 Image Analysis

The Image analysis was performed in Python (Version: 3.10, Python Software Foundation, Wilmington, Delaware, USA.) in a scientific environment (Miniconda, Version: 24.5.0, Anaconda, Inc., Austin, Texas, USA.) with Spyder (Version: 6.1.0, Pierre Raybaut, USA.). Aside from the standard packages of Miniconda that were used for basic mathematical operations, NumPy and SciPy, PoreSpy were used to calculate pore coordinates and local thicknesses (Har-

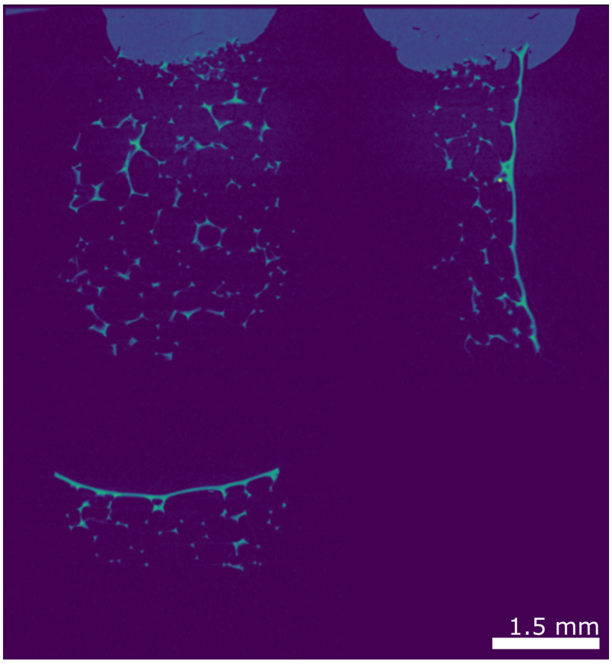

Figure 4: Orientation of reconstructed scans for beam thickness and cell spacing analysis.

ris et al., 2020; Virtanen et al., 2020; Gostick et al., 2019). All utilized scripts will be provided on request.

The goal of the image analysis is to provide the data needed for the algorithm. For this, it has to be a measure for the gradient of the beam thickness and cell spacing along the radius of the cocoon. The radius of the cocoon was measured in % with 0 % representing the inner and 100 % the outer radius. PoreSpy's local thickness used as the measure for beam thickness, which is only proportional to the actual beam thickness and cannot be used as a quantitative measure. Since the absolute beam thickness values of the algorithm will be determined by the user through $ThicknessScalar$, this was deemed sufficient.
The analysis is based on the assumption that the radial coordinate does not change its angle depending on the position in the volume and therefore corresponds to one of the cartesian coordinates. This assumption was made, because the length of the wall sections is small compared to the radius of the cocoon and the inside of the wall was rotated to face one of the cartesian coordinates.
Each scan was prepared for analysis in the same way. First, a scan was imported and rotated to match the orientation shown in Figure 4. That way the radial axis always points in the same direction. Then it was transformed into a binary volume with a threshold of 0.3. Next, the region of interest (ROI) was determined manually as the largest section that had been unaffected by the preparation process by displaying the scan in different orientations and excluding collapsed cells and broken beams. Then, all coordinates were divided by the total length of the ROI in the radial axis, to make all values relative to the wall thickness, as the algorithm requires.
After preparation, the beam thickness and cell spacing of each binary volume was analyzed. The beam thickness analysis saves a value pair of the radial coordinate and the corresponding local thickness for each voxel that exists along the radial axis. The local thickness value of one these radial voxels was calculated by averaging all local thickness values of every voxel in the plane

perpendicular to the radial axis that crosses said radial voxel. This reduces one beam thickness corresponding to three cartesian coordinates down to one beam thickness corresponding to one radial coordinate. Done for all radial voxels, a full gradient of the beam thickness along the radius is achieved.

For the cell spacing analysis the pore network of the binary volume was calculated with the implementation of Sub-Network of an Over-segmented Watershed (SNOW)-network extraction of PoreSpy. Coordinates of cells (= pores) are a part of the data of networks calculated this way. For each cell, the distance to the nearest cell neighbour was calculated using the KD-tree functionality of SciPy from the cell coordinates. This value was taken as a measure for the cell spacing and one of its cartesian coordinates as its radial position, as dictated by the assumptions made.

Initially, a data set was created from the scan of only one cocoon to create the model for the evaluation of the FEA. Later, more data was collected and averaged for a closer reproduction of the average gradient of leech cocoons. To be able to average out beam thicknesses and cell spacings with different radial values across multiple cocoons, each scan was fitted with a curve. The beam thickness curves were fitted with a simply cubic spline interpolation with continuation extrapolation. Because the cell spacing data was noisy by nature, due to the inherent randomization of cell coordinates of Voronoi lattices, the UnivariateSpline class of the SciPy package was used, which uses a Generalized Cross-Validation (GCV) algorithm to calculate a smoothing factor (Craven and Wahba, 1978). Continuation extrapolation was used here as well. Finally, the means and standard deviations of the values of every curve were calculated at 100 equally spaced radii for both beam thickness and cell spacing. The resulting average beam thickness and cell spacing represents the result of the image analysis and was integrated into the lightweighting algorithm.

2.4 Lightweighting

2.4.1 Algorithm Creation

The structure of the cocoon is abstracted into two main components: An inner closed wall and an outer Voronoi lattice that exhibits a radial gradient of its beam thickness and cell spacing. Further Inwards from the closed inner wall, the cocoon is completely hollow.

The algorithm was based on this abstraction and generates an output geometry from any given input geometry. By creating it in nTop (Version: 5.33.3, nTopology, Inc., New York, New York, USA.), the creation of these intricate geometries is made possible through its implicit modeling capabilities.

The output geometry should reflect all previously named aspects of the cocoon structure, while also remaining adjustable to the user's needs. Four different input variables may be provided to control the output: $InputGeometry$, $WallThickness$, $BeamThicknessScalar$ and $CellSpacingScalar$ (s. Table 1). $InputGeometry$ is the geometry that the algorithm will be applied to and the outer shape of the output geometry will be identical to it. $WallThickness$ determines the thickness of the entire cocoon wall (inner wall and Voronoi lattice combined). Everything further inside will be completely hollow. $BeamThicknessScalar$ and $CellSpacingScalar$ determine the properties of the Voronoi Lattice. They allow making the Voronoi lattice lighter or heavier, despite it having predetermined gradients. Adjusting them will keep the gradi-

Table 1: Input variables of the algorithm with their effects on the output. This overview may serve as orientation for anyone attempting to apply the algorithm themselves.

Variable	Type	Effect
InputGeometry	Implicit Body	Determines geometry to apply the algorithm to
WallThickness	Scalar	The higher, the heavier/stiffer is output
BeamThicknessScalar	Scalar	The higher, the heavier/stiffer is output
CellSpacingScalar	Scalar	The lower, the heavier/stiffer/more complex ...

ent the same relatively, while changing the total amounts. All internal variables are relative to *WallThickness* or *InputGeometry*, to allow for maximum flexibility. The algorithm also converts *BeamThicknessData* and *CellSpacingData* from external files into Table blocks to determine gradients based on those found in the cocoons of leeches, but these data are not intended to be adjusted in the scope of this thesis, since they represent an aspect intrinsic to the leech cocoon structure.

The algorithm is created as an nTop-workflow consisting of its internal blocks in the following order:

1. **Input:** *InputGeometry*, *WallThickness*, *ThicknessScalar*, *SpacingScalar*, *BeamThicknessData* and *CellSpacingData*
2. Shell: *CocoonWall* from *InputGeometry* with *WallThickness* as thickness.
3. Field: *BeamThickness* from transferring *BeamThicknessData* to *InputGeometry*
4. Field: *CellSpacing* from transferring *CellSpacingData* to *InputGeometry*
5. VoronoiLattice: *VoronoiLattice* from random Points inside *CocoonWall* with *CellSpacing* as point distance and with *BeamThickness* as beam thickness
6. BooleanSubtract: *CocoonInside* from *InputGeometry* - *CocoonWall*
7. Scalar: *InnerWallThickness* from evaluating the first data point of *BeamThicknessData*
8. Shell: *InnerWall* from *CocoonInside* with *InnerWallThickness* as thickness
9. BooleanUnion: *OutputGeometry* from *VoronoiLattice* + *InnerWall*
10. **Output:** *OutputGeometry*

2.4.2 Geometry Creation

Four different categories of geometries were created from different thin-walled input geometries for different purposes. A summary can be found in Table 2. Within each category, multiple different geometries were created, by applying a different lightweighting process. Sometimes the cocoon-inspired algorithm with differing input data was applied, other times a simple uniform shell operation was performed to create a comparison at approximately the same mass. For each, the input variables *ThicknessScalar* of 5, a *SpacingScalar* of 3 and a *WallThickness* of 5 mm were used. These values produced geometries that had a comparable amount of cell rows

Table 2: Categories of created geometries along with the input geometries they were based on and their purpose.

Category	Input Geometry	Purpose
Suzanne	Monkey primitive	Algorithm showcase
Curved	Cylinder section	Compression tests and FEA
Edged	Cube edge	FEA
Flat	Cube face	Image analysis/algorithm validation

along the radius as the leech cocoons and kept beams thick enough to produce them in additive manufacturing. A full list of all geometries and their input data can be found in Table 3. The input geometry for the Suzanne category was created in Blender (Version: 4.1.0, 2024, Blender Foundation, Amsterdam, Netherlands) by remeshing the monkey primitive and then imported into nTop. The purpose of this geometry is to verify the claim that the algorithm can be applied to any geometry, even if it has complex features.

Table 3: List of all geometries along with the input data used to create them. If the input data is listed as None, it was created by performing a simple uniform shell operation. Else it was created by applying the cocoon-inspired algorithm.

Geometry List	Input Data ($CellSpacingData/BeamThicknessData$)
Suzanne	Cocoon Average
Curved Cocoon Comparison	Single Cocoon Measurement
Curved Cocoon	Cocoon Average
Curved Shell	None
Edged Cocoon	Cocoon Average
Edged Shell	None
Flat Constant	Manufactured Constant
Flat Linear	Manufactured Linear

The masses of all geometries were compared to the input geometry that had a uniform shell operation performed on it with the same $WallThickness$ used as an input variable for the algorithm of 5 mm. Masses were calculated using the Mass Properties and mass reduction with the Weight Savings block in nTop. For this the named density in the data sheet of Bambu Lab's PLA Basic of $1240\,\mathrm{kg\,m^{-3}}$ was used (Bambu Lab, n d). To have the ability to effectively produce them with additive manufacturing, all geometries, except Suzanne, were scaled up by a factor of 3.

2.5 Finite Element Analysis (FEA)

Five FEA were conducted in total. Their names and goals are described in Table 4.

Table 4: List of all FEA along with their purpose.

Simulation	Goal
Curved Cocoon Comparison	Comparison to compression tests
Curved Cocoon Buckling	Examination of buckling of Curved Cocoon
Curved Shell Buckling	Comparison to RBL of Curved Cocoon and compression tests
Edged Cocoon Buckling	Examination of buckling of Edged Cocoon
Edged Shell Buckling	Comparison to RBL of Edged Shell

All of them were conducted using the same setup that was slightly adjusted to fit the varying

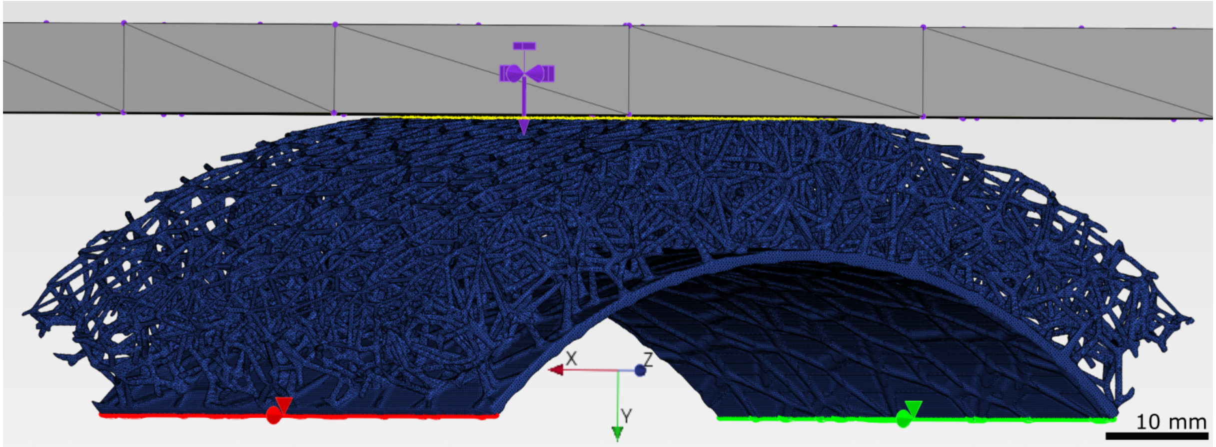

Figure 5: Boundary Conditions of the FEA demonstrated on the Curved Cocoon Comparison Simulation. The upper geometry is the compression implement (grey), while the compressed part is the lower geometry (blue). Displacement and rotation constraints are represented by coloured arrows and cuboids respectively. On the bottom left and right of the curved part is a fixed displacement in the y and z-axis (red and green). The entire upper compression implement has a displacement in the y-axis of 5.3 mm and fixed displacement in both the x and z axis, on top of fixed rotation in all three axes (purple). A tie knot constraint exists between the lower surface of the compression implement and upper nodes of the compressed part (yellow).

models. Any geometries used represent a section of a thin walled structure that may be mirrored to recreate it in its entirety. This is done to reduce compute time. The models were created and exported with the meshing tools of nTop. The element type used for the FE-meshes of the compressed geometries was tetrahedral (Tet4) and with an edge length of 0.4 mm. Element sizes were kept constant across the entire geometry, since every small beam could represent a point of failure. This lead to element counts ranging from 2.7 to 4.8 million. The mesh for the compression implement was kept as rough as possible with 122 Tet4 elements with an edge length of 40 mm, since its only purpose was to apply the load evenly. The FE-meshes were imported into PrePoMax (Version: 2.4.0, Matej Borovinšek, Maribor, Slovenia), where the boundary conditions were added and the simulations were solved with the PaStiX solver. All Boundary conditions can be found in Figure 5. The time simulated was 1 s of automated incrementation with an initial time increment of 0.2 s and a maximum of 20 increments.

The simulations mimic a radial compression of parts by a large compression implement. From the compression tests it was determined that the compressed geometry's RBL occurred at a displacement of 5.3 mm, after which the part bends and the measured forces no longer increased. Because of this, all parts were simulated with a displacement of the compression implement up to this exact displacement. The maximum reaction force at the bottom restrictions of the compressed part taken together represent the result of the simulated RBL.
All material properties can be found in Table 5. The Material of the implement was defined as

Table 5: Material properties used in every FEA.

Material	Young's Modulus	Poisson's Ratio	Yield Stress	Yield Strain
Steel	210 000 MPa	0.3	/	/
PLA	2370 MPa	0.36	35 MPa	0.0148

steel with elastic properties. Its young's modulus was chosen as 210 000 MPa and its Poisson's ratio as 0.3. The material of the compressed parts were based on PLA (PLA Basic, Bambu Lab, Shenzhen, China) according to the official data sheet (Bambu Lab, n d). To more accurately simulate the large strains the material was subjected to, elastic-plastic material properties were chosen. The lowest named young's modulus of 2370 MPa was used to keep the simulated RBL on the lower end. The chosen yield stress of 35 MPa was based on the minimal tensile strength given in the data sheet and the yield strain of 0.0148 was calculated by dividing the yield stress by the young's modulus. The Poisson's ratio of 0.36 was based on Farah et al. (2016).

2.6 Validation

2.6.1 Compression Tests

To verify FEA results, two compression tests with a sample size of six each were conducted. The two different geometries used were the Curved Cocoon Comparison and the Curved Shell. For this purpose, all twelve specimens were manufactured with a 3D-printer (P1S, Bambu Lab, Shenzhen, China) with a nozzle diameter of 0.4 mm out of PLA (PLA Basic, Bambu Lab, Shenzhen, China). The system preset "0.12mm High Quality BBL X1C" with a layer height of 0.12 mm with minor adjustments and the filament preset "Bambu PLA Basic @BBL X1C" with a printing temperature ranging from 190 °C to 240 °C were used. The deviating settings are shown in Table 6. The printing orientation was such that one end of the specimen sat flush on the print bed. The specimens were stored and tested at an ambient temperature of around 23 °C and a humidity of around 50 %. Directly before compression, the masses of all specimens were measured using a laboratory scale (EMB 200-3, KERN & SOHN Gmbh, Balingen, Germany).

The setup closely resembled that of the FEA shown in Figure 5, but with an additional implement on the bottom of the compressed specimen, instead of the displacement constraints. A universal testing machine (Tensile Tester Z020, ZwickRoell Group, Ulm, Germany) was used at a testing speed of 5 mm min^{-1}. The compression implements were custom made to fit probes with a square base measuring 10 mm×10 mm. The starting distance between the implements was 35 mm and the test ended at a distance of 10 mm. The data recorded from the machine was force in N, displacement in mm and time in s. All tests were recorded using a phone camera (Skyline, HMD, Espoo, Finnland) that was mounted to the machine.

Table 6: 3D-printing settings used to produce all specimens that deviate from the system preset "0.12mm High Quality BBL X1C".

Setting	Value
Sparse infill	100 %
Sparse infill pattern	Rectilinear

Setting	Value
Enable support	Yes
Brim type	Outer and inner brim

2.6.2 Reapplication of Image Analysis

To verify the accuracy of the lightweighting algorithm and the image analysis that produces the data that it reads, two custom beam thickness and cell spacing data were manufactured that consist of perfectly constant and linear gradients respectively. These data were used as the beam thickness and cell spacing gradients of the algorithm to produce the two geometries Flat Constant and Flat Linear. One should have perfectly constant, and the other perfectly linear beam thickness and cell spacing. Then, the two geometries were read as binary volumes and the

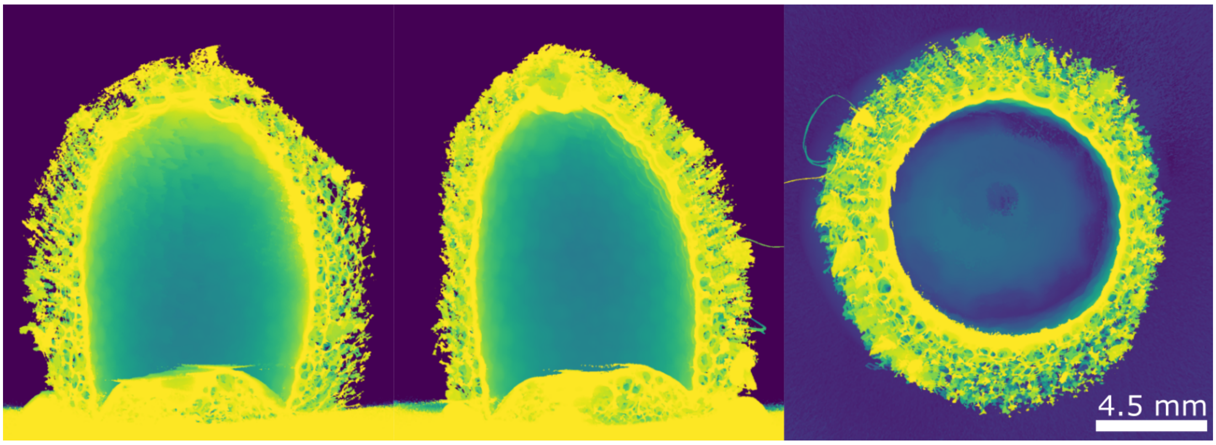

Figure 6: Cross section of the full, fresh cocoon scan from three different perspectives. From left to right are the perspectives front, side and top. In all three perspectives, afterimages are visible, making the image appear blurry. This was caused by the rapid shrinking of the specimen during scanning. Specifically at the upper right of the cross section in the middle, the inner wall is visible twice, making it appear very thick at first glance. Furthermore, at several sections, larger spots of full volume are visible that obscure the underlying structure. On top of this, the lower cocoon has been damaged and has buckled inwards. These factors are unfavourable for an accurate analysis of the delicate Voronoi structures

image analysis was applied to them. The results were then compared to the manufactured input data that was scaled by a constant factor, because the goal is to accurately measure the relative gradient, not measure its absolute values. The cell spacing input data was scaled, so that the data point at a radius of 0 % matches the output data, while the beam thickness input data was scaled, so that the data point at 20 % matches the output data. This difference in approach was chosen, because the image analysis proved accurate at different radii for cell spacing and beam thickness analyses. Any deviation from the scaled input data functions represent an error of the methodology used to generate the algorithm.

The noise that is intentionally introduced to randomize the cell positions for the Voronoi lattice was also validated. For this, the root mean squares (RMS) of the residuals of the smoothed splines created from the cell spacing data were calculated for both the biological measurements and the measurements gathered from the Flat Constant geometry. These RMS represent the average deviation of data from the spline and are thus used as a measure for noise. The RMS of the biological samples was then scaled the same way as the cell spacing measurement to validate the relative accuracy.

3 Results

3.1 CT-Scanning

The fresh cocoon reacted very quickly with the lower humidity in the CT-Scanner and deformed during scanning. Because they were still moist, cleaning off residue substrate proved difficult without damaging the delicate wall structures. During preparation, the fresh cocoons were also much less stiff, making them easily damaged in the process. This lead to a low quality scan that can be found in Figure 6. The difficulties made it apparent that the methodology is not suitable to produce a quality of scans high enough for an accurate image analysis of fresh cocoons.

Thus, the focus was shifted towards only the dried cocoons. The scans produced with the same methodology on a full dry cocoon showed no clear defects and can be found in Figure 7. The characteristic closed inner wall surrounded by a lightweight outer Voronoi lattice were found intact.

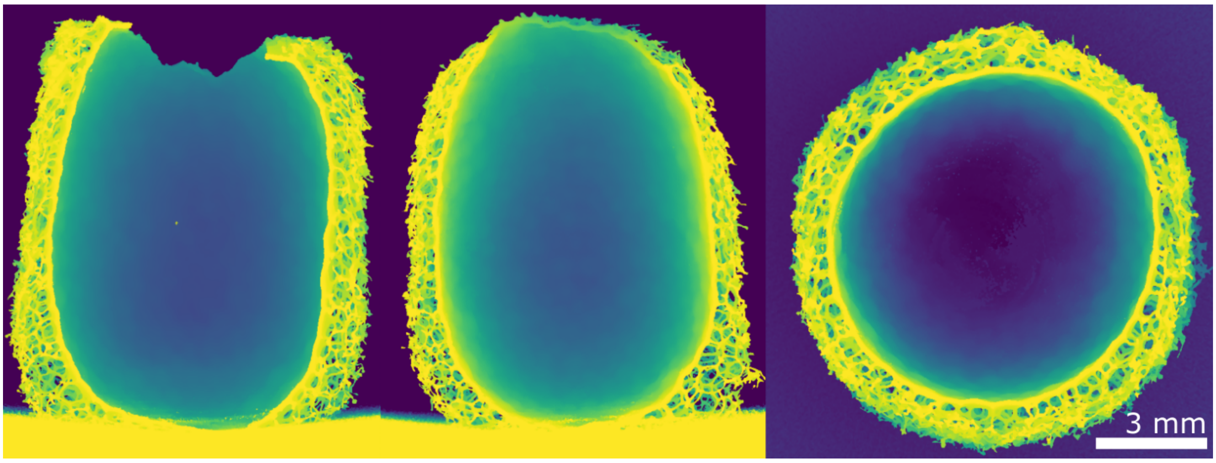

Figure 7: Cross section of the full, dry cocoon scan from three different perspectives. From left to right are the perspectives front, side and top. The thickness of the walls seems to show differences in the front and side view, while it appears to be similar in the cross section from the top view. Clearly visible is the fully closed inner wall and the outer open cellular structure.

The scans of small wall segments consisted of an interconnected network of thin beams that make up cells of varying shape and size. Representative sections can be found in Figure 8.

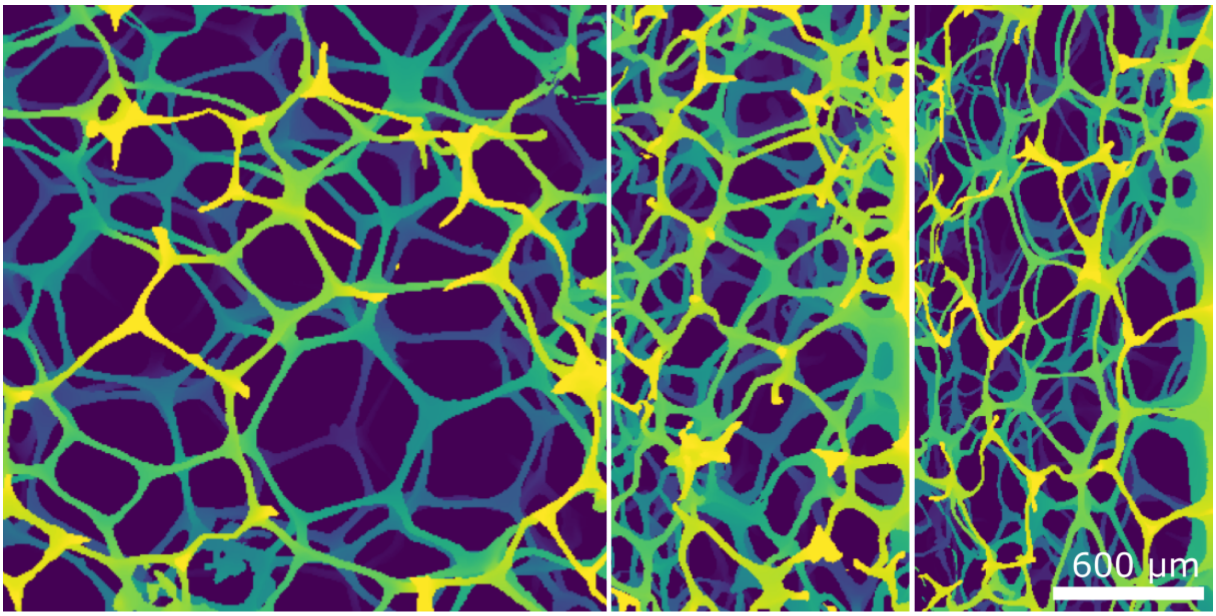

Figure 8: Scans of a dry cocoon wall section specimens used for image analysis from three different perspectives. From left to right are the perspectives front, side and top. All perspectives are from different specimens that were selected to represent the typical structure. The characteristics of a three dimensional Voronoi structure are represented. Visible are the thin beams interconnected in all three dimensions that create a rigid structure, even when taking up only a small part of the volume. The sizes and geometries of these cells do not appear to adhere to a periodical structure, like is the case for Voronoi structures. These characteristics are shared between all perspectives.

3.2 Image Analysis

The image analysis produced the average beam thickness and cell spacing gradients over the radius from the image slices of the ten small wall section specimens found in Figure 9. The beam thickness showed an initial area with two local maxima until a radius of 20 %, after which it mellows out into an almost linear area with a shallow downward slope. Its standard deviation showed a decrease along the radius. The cell spacing curve appears similar to a section of a negative quadratic function with relatively high standard deviations that show the same decrease as those of the beam thickness.

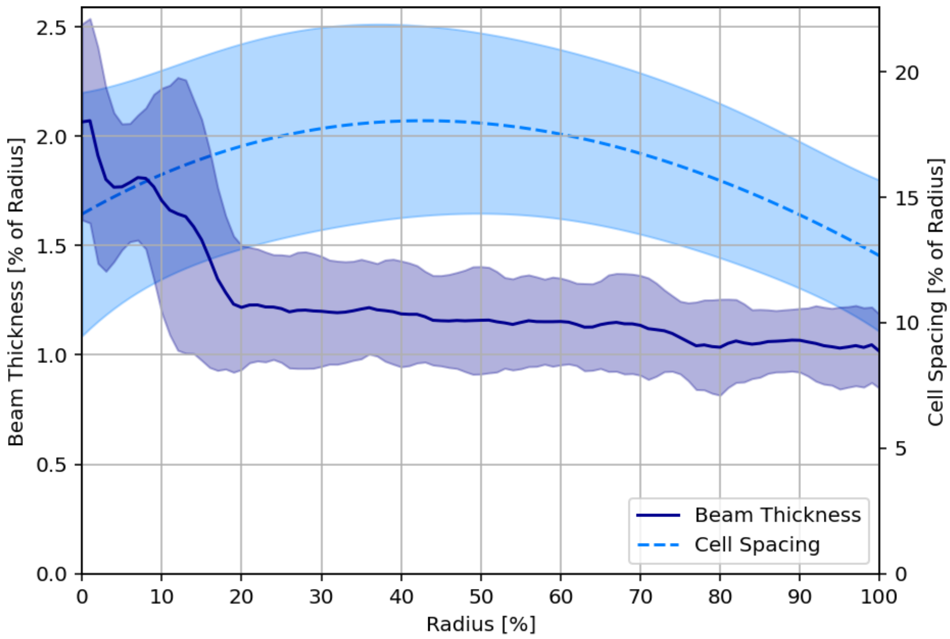

Figure 9: Average beam thickness and cell of the ten wall section specimens. The colour-coded error area represents the standard deviation. The beam thickness curve shows an initial section with two local maxima. At a radius of 20 %, the values are decreased drastically and a near linear decrease with a shallow gradient follows. Its standard deviation is higher initially and decreases further along the radius. The cell spacing curve resembles the shape of a section of a negative quadratic function. It starts slightly higher than it ends. Its standard deviation also shows a decrease along the radius, but is relatively much higher than that of the beam thickness curve.

3.3 Lightweighting

Geometries produced by the application of the cocoon-inspired algorithm reflected the characteristics found in the scans of the cocoons. It could be applied to any geometry, even those with more complicated features. This is demonstrated on the lightweighting of the Suzanne geometry found in Figure 10.

With the input variables used, it produced mass reductions ranging from 81.8 % to 83.9 % with the input data derived from the image analysis. With the manufactured constant and linear input data, it lead to a mass reduction of 70.3 % and 78.0 % respectively. This shows that the input data has an effect on the properties of the algorithm. That the constant input data produced a lower mass reduction than the linearly decreasing input data is also in line expectations, considering that both started at the same value. The full results are listed in Table 7.

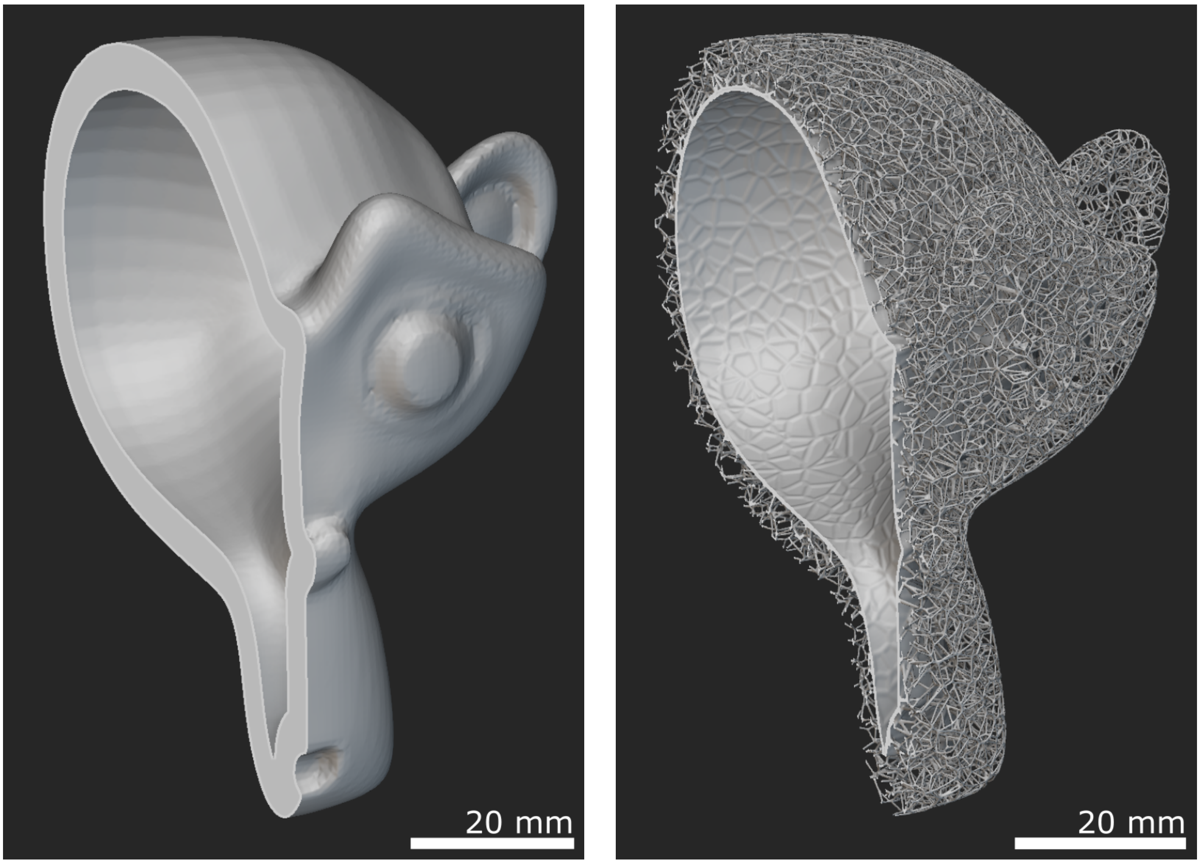

(a) (b)

Figure 10: Cross section of the lightweighted Suzanne geometry. In (a), the base geometry is shown. It takes the shape of a stylized monkey with many distinct features. Depicted in (b) is the output geometry after applying the cocoon-inspired lightweighting algorithm. The other bounds remain the same and the features are represented, although much less clearly visible. Cocoon-like aspects such as the inner wall and outer Voronoi lattice are visible.

Table 7: Results of the lightweighting process for each Geometry

Geometry	Mass [g]	Mass Reduction [%]
Suzanne	13.0	83.2
Curved Cocoon Comparison	23.9	83.9
Curved Cocoon	27.0	81.8
Curved Shell	27.0	81.8
Edged Cocoon	25.5	82.7
Edged Shell	25.5	82.7
Flat Constant	31.0	70.3
Flat Linear	22.9	78.0

3.4 FEA

A full list of the numeric results of the FEA in regards to the RBL can be found in Table 8.

Table 8: Numeric results of the FEA for each Simulation. The mass of the compressed geometry is provided again to show that not every simulation can be compared equally.

Simulation	Mass [g]	RBL [N]
Curved Cocoon Comparison	23.9	317.3
Curved Cocoon Buckling	27.0	310.3
Curved Shell Buckling	27.0	133.1
Edged Cocoon Buckling	25.5	239.0
Edged Shell Buckling	25.5	125.4

According to the FEA, the geometries that had the cocoon-inspired algorithm applied to them showed far higher buckling loads than the one's produced with a uniform shell operation, although the difference was smaller for the edged geometries compared to the curved geometries. However, it has to be added that the displacement of the implement was much smaller for the Edged Cocoon FEA, since the simulation reached the maximum increments due to excessive deformation of elements in the area of cotact to the compression implement. The final implement displacement calculated was 3.9 mm of the intended 5.3 mm. This was not evaluated as a failure when estimating the RBL, because the plateau of the reaction force occurred even earlier at an implement displacement of 2.7 mm.
Remarkably so, the Curved Cocoon Comparison geometry, which was created with the cocoon-inspired algorithm from input data of only one wall section specimen, showed the highest RBL at 317.3 N despite consiting of the lowest mass at 23.9 g.

A direct comparison of the final increments of the FEA of the Curved Cocoon and Curved Shell geometries is shown in Figure 11.

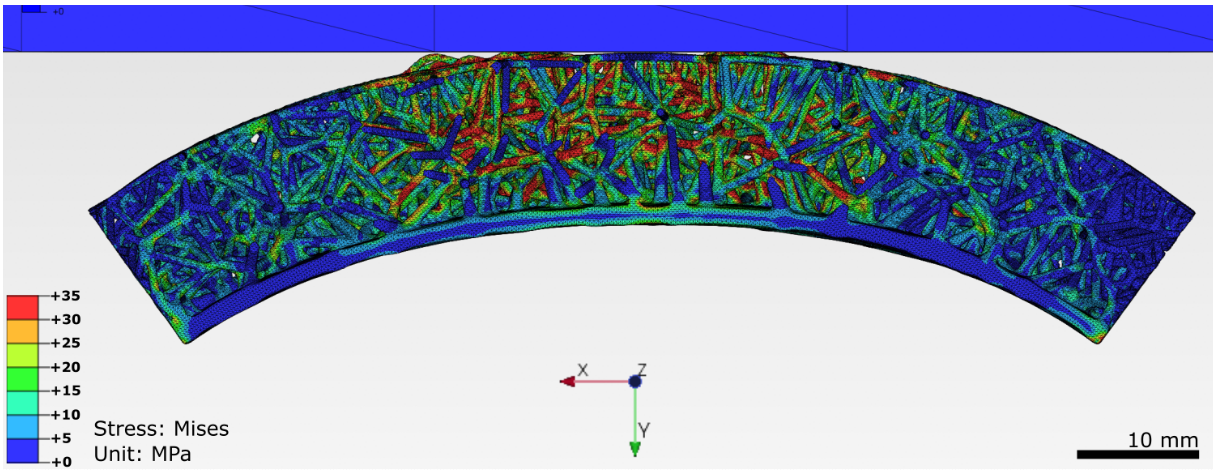

(a)

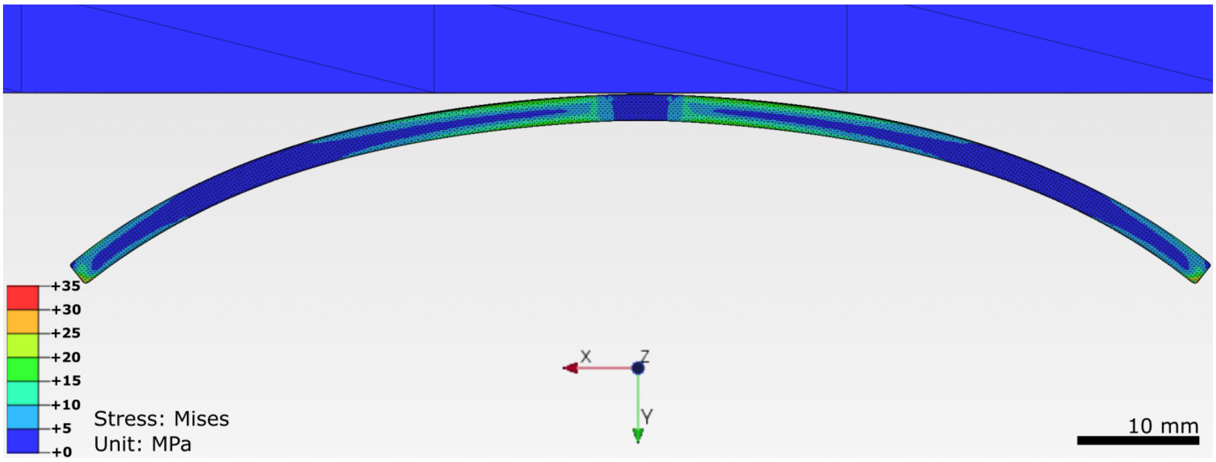

(b)

Figure 11: Comparison of the FEA of the Curved Cocoon (a) and Curved Shell (b) Geometries. The overall shape of the deformation is similar between the geometries, though some beams have bent outward in the upper bounds of the Curved Cocoon geometry. The stresses in the upper region are much higher in the small beams of the Curved Cocoon than in the full material of the Curved Shell, reaching the yield stress of 35 MPa. In fact, it seems like in the upper part of the Curved Shell, there is no stress at all. The distribution of stresses appears to me more uniform in the Curved Cocoon across the material and also radiate into the inner wall, while they seem to be more concentrated on the inner and outer regions of the upper and lower areas in the Curved Shell.

Both geometries seem to follow the same overall deformation on a surface level. The Von Mises stresses seemed much higher and more equally distributed for the Curved Cocoon geometry than in the Curved Shell geometry. This is in accordance with the RBL being much higher for the Curved Cocoon geometry, despite having the same total mass.

A similar comparison, but between the Edged Cocoon and Edged Shell geometries, can be found in Figure 12.

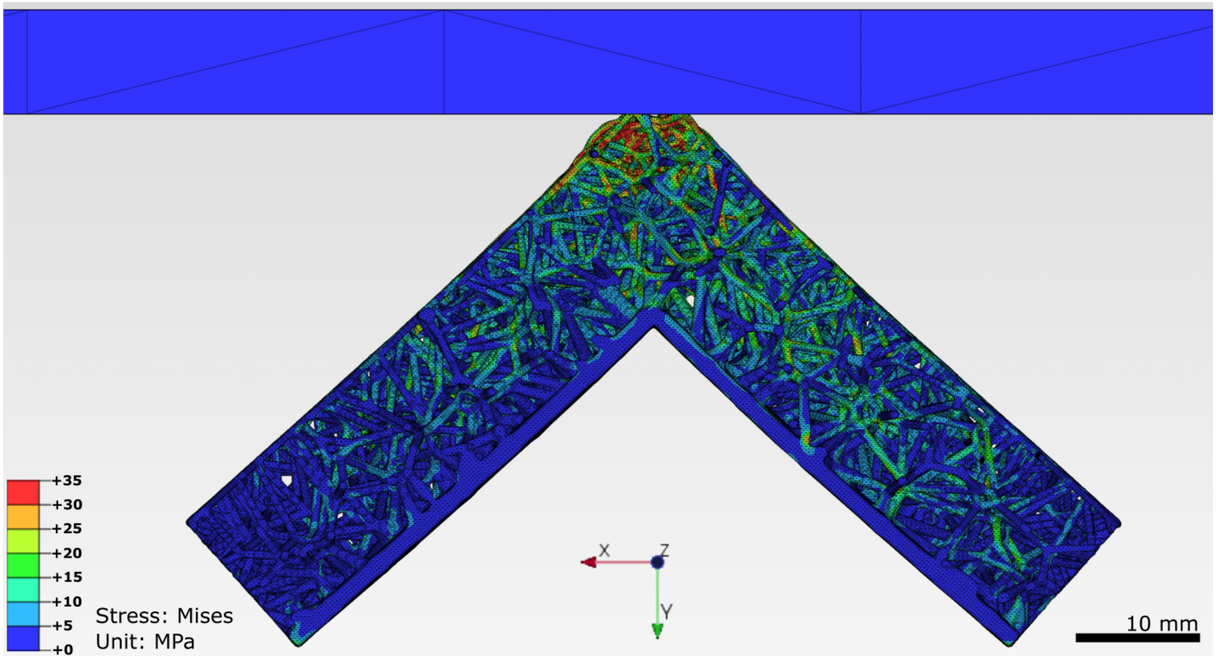

(a)

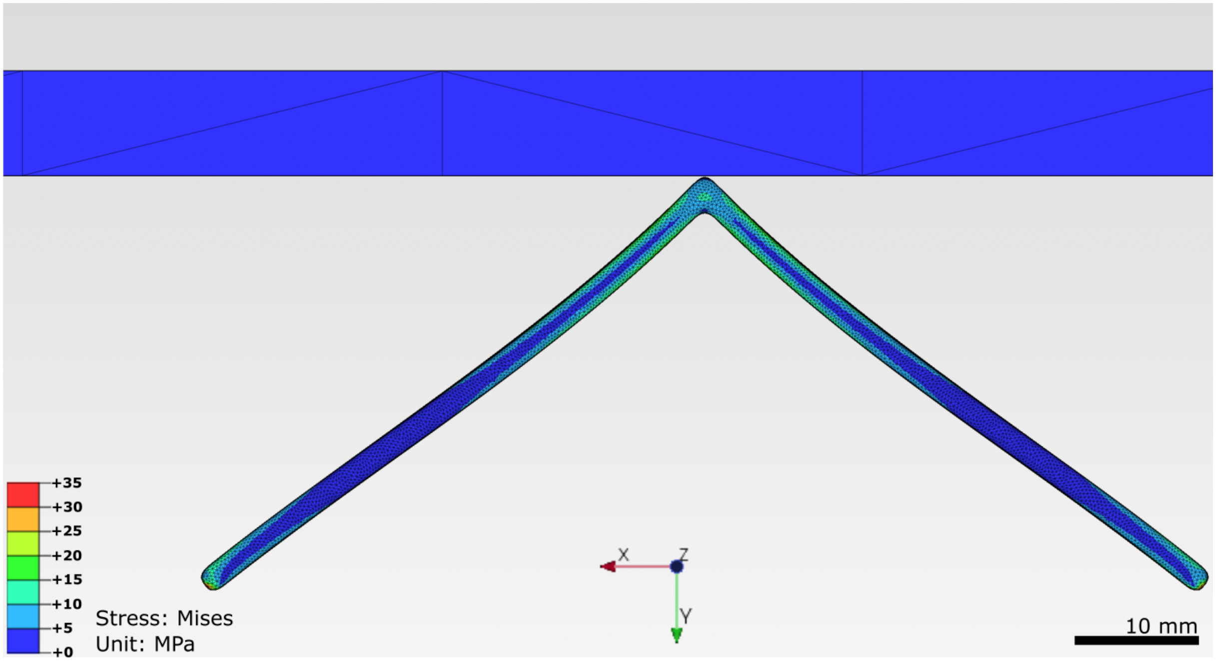

(b)

Figure 12: Comparison of the FEA of the Edged Cocoon (a) and Edged Shell (b) Geometries. The displacement of the implement in the Edged Cocoon is lower, as the simulation stopped early. Deformation seems to be much more concentrated to the contact are with the implement for the Edged Cocoon, while the Edged Shell shows bending further downwards. The Edged Cocoon shows the highest stresses heavily concentrated at the contact point to the implement. Lower stresses radiate into a large portion of the Voronoi lattice, but fail to reach the vast majority of the inner wall.

Here, the shape of the deformation of the two bodies deviated. The deformation of the Edged Cocoon seemed to be much more concentrated on the contact area of the geometry to the compression implement, which caused the excessive deformation leading to the early termination of the simulation. Stresses did not get distributed into the inner wall here, unlike the Curved Cocoon geometry. Despite the implements being much further displaced, the Edged Shell still had much lower maximum stresses compared to the Edged Cocoon. This is still in line with the observation that the reaction forces are also lower here compared to those of the Edged Cocoon.

3.5 Validation

3.5.1 Compression Tests

Both the compression tests and the FEA showed similar trends qualitatively. The RBL measured for the geometry created by applying the cocoon-inspired algorithm is far higher than the one created by performing a simple uniform shell operation. The discrepancy compared to the FEAs absolute force values is remarkably high however. The RBL, taken from the force of the final increment or measurement at 5.3 mm, showed a discrepancy by a factor of 2.27 for the Curved Cocoon Comparison and of 3.39 for the Curved Shell geometry. Unlike the higher RBL suggest, the Curved Cocoon Comparison specimens showed a considerably lower average mass of 19.6±0.04, compared to the Curved Shell's 23.7±0.02. Both masses were lower than the expected masses calculated in nTop for the geometries. The exact values can be found in Table 9.

Table 9: The RBL measured in the compression tests, along with the mass of the 3D-printed specimens, compared to the RBL measured in the FEA.

Specimen	Mass [g]	Measured RBL [N]	Simulated RBL [N]
Curved Cocoon Comparison	19.6±0.04	139.7±1.60	317.3
Curved Shell	23.7±0.02	39.3±0.38	133.1

The specimen after compression are shown in Figure 13. The Curved Cocoon Comparison specimen shows a deformation of the Voronoi structure and recovered its curvature partially, while the Curved Shell geometry recovered fully. This is caused by the former being much thicker, meaning its wall was compressed much further at the same implement distance. The recovery shows that the specimens were highly flexible.

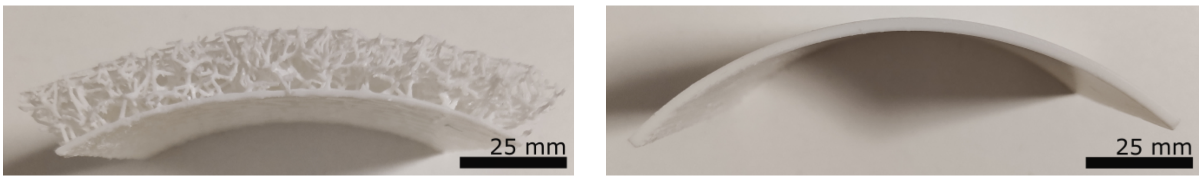

(a) (b)

Figure 13: Specimens after compression. In (a), a Curved Cocoon Comparison specimen after compression is shown, while (b) depicts a Curved Shell specimen. The specimen in (a) shows a compressed wall and a slight recovery of the curvature. For the specimen in (b), the curvature seems to be fully recovered.

A comparison of the curves from 0 mm to 5.3 mm is depicted in Figure 14. Despite the large discrepancy of the absolute values, the general shape of the FEAs results are also reflected in the results of the compression tests. Both curves of the Curved Cocoon Comparison start with a steep, near linear incline, that quickly levels out to a near plateau state. The curves of the Curved Shell comparison show a much shallower incline, but also a far less pronounced flattening, appearing near linear.

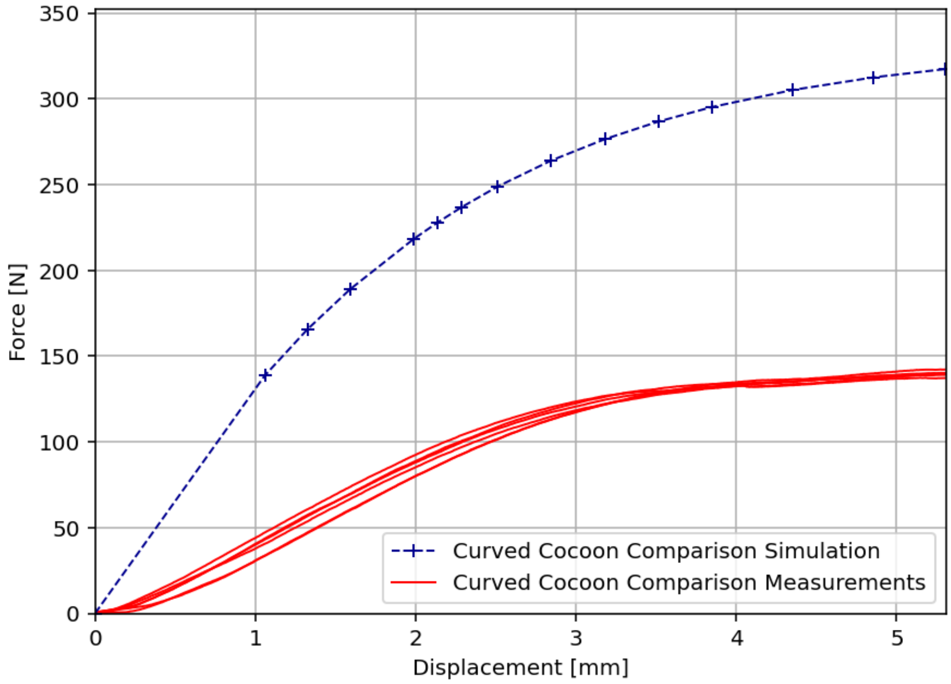

(a)

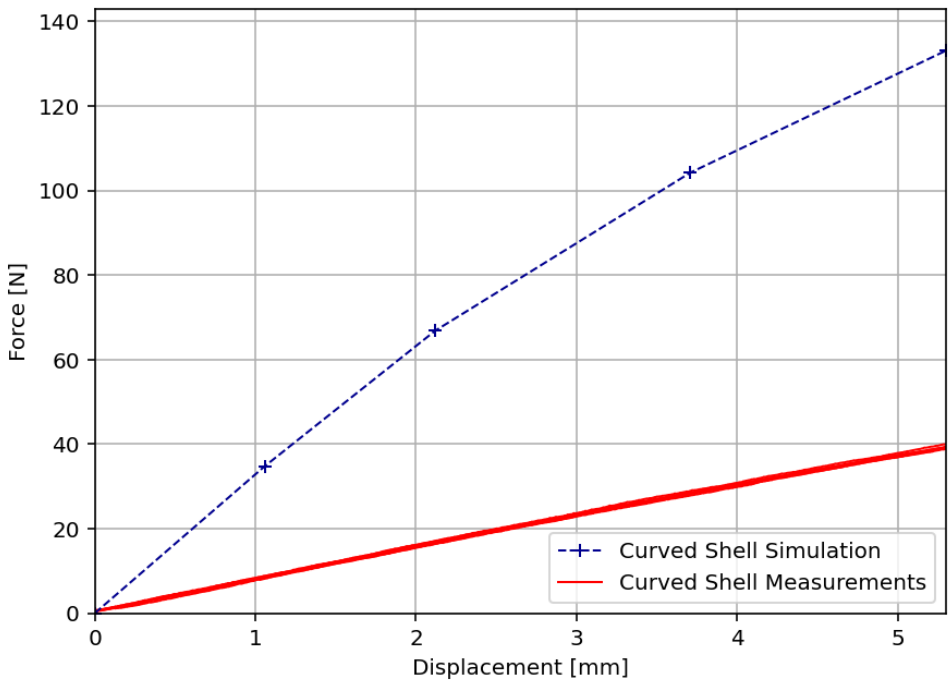

(b)

Figure 14: Comparison of the compression tests results compared to the FEA Simulation. Depicted in (a) is the comparison for the Curved Cocoon Comparison geometry. The measurement curves appear very similar, only showing minimal deviations in the initial section. The simulation and measurements show a similar general shape, though the absolute values found at the final displacement of 5.3 mm differ by a factor of 2.27. In (b), the same is shown for the Curved Shell geometry. Here, a similar trend is visible. The curves of all six measurements are so close together, that they appear as if they were one line. The general shape of both curves is a near linear increase with a slight negative curvature. Again, the simulation produced much higher forces, this time by a factor of 3.39.

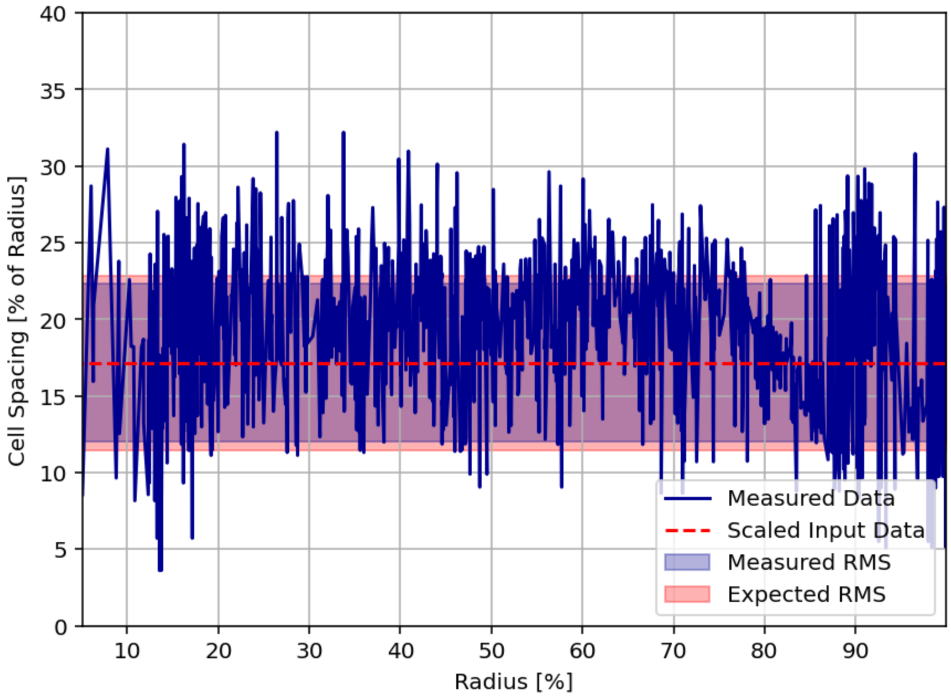

Figure 15: Validation of the cell spacing noise measured in the Flat Constant geometry. The RMS are shown as error areas around the constant, scaled input data. The measured data appears to be random white noise around the constant input data curve. The measured RMS closely reflects the expected RMS calculated from the cell spacing data of the biological specimens.

3.5.2 Reapplication of Image Analysis

The RMS measured from the Flat Constant geometry is almost identical to the expected RMS calculated from the data of the biological specimen (s. Figure 15). This shows that the randomization of the cell positions of the Voronoi lattice produced by the cocoon-inspired algorithm closely resembles that of the actual leech cocoons.

From the reapplication of the Image Analysis on flat geometries created by the cocoon-inspired algorithm with manufactured data, the error of the process used to create the cocoon-inspired algorithm is shown. The expected trends are still reflected in the results, despite clear deviations at certain sections (s. Figure 16). The process for cell spacing seems to introduce a curvature from the completely straight input data, despite generally following the input data at the beginning and end. For beam thickness, large sections could be almost completely reproduced. The outer edges, especially at the lowest radii, deviate greatly, however, and show a pattern similar to that found in the averaged beam thickness data measured from biological specimens.

4 Discussion

The used methodology proved unsuitable for the analysis of fresh cocoons. To accomplish this, a controlled environment would have to be created that protects the specimens from external conditions. Despite this, the complications hint at unexplored properties of the complex structures of *Hirudo sp.* cocoons. They very quickly reacted to a more arid environment and seemed

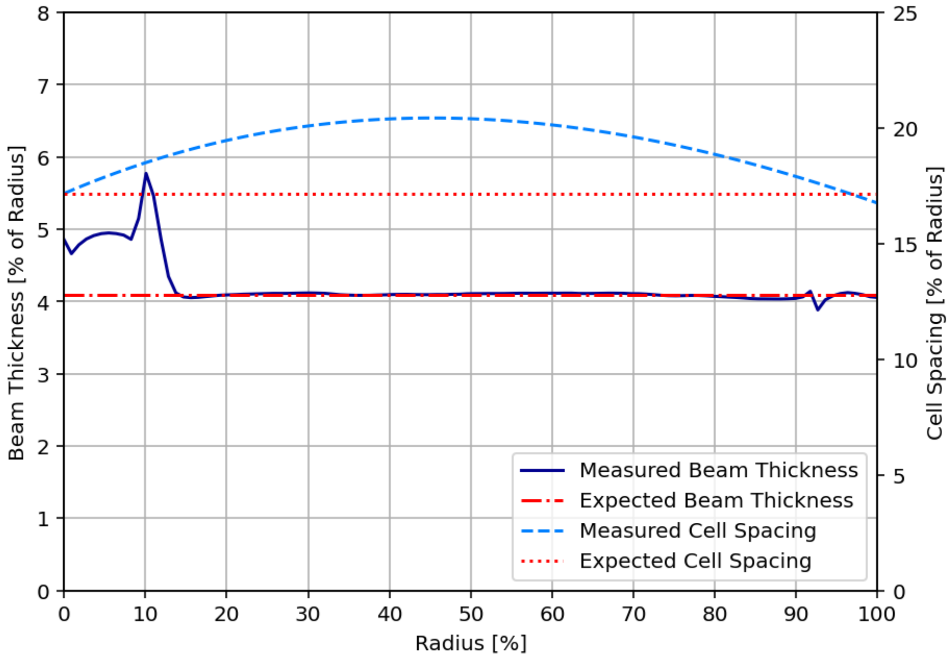

(a)

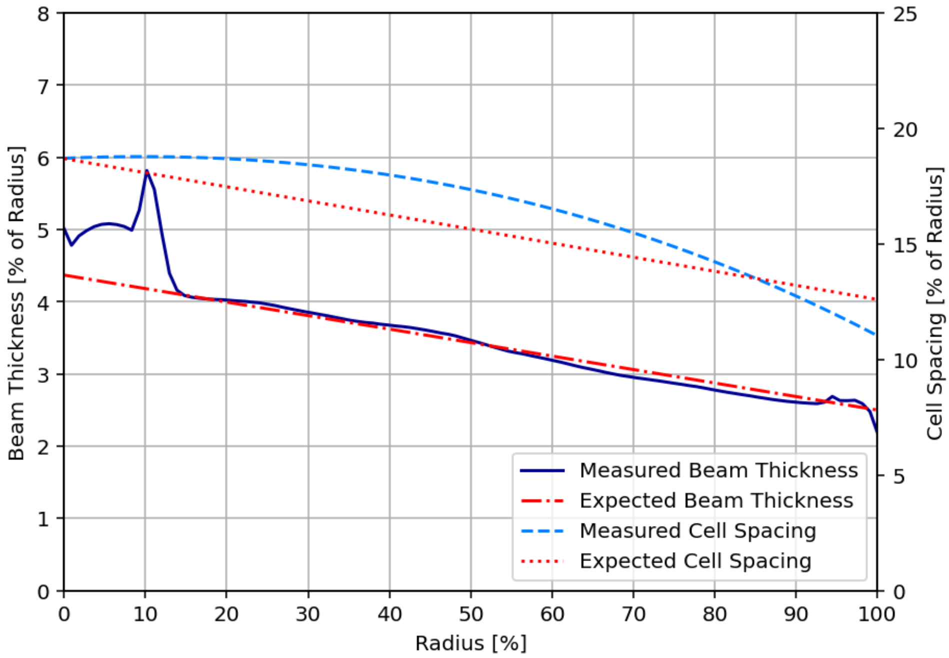

(b)

Figure 16: Validation of the cell spacing and beam thickness produced by the algorithm and measured by the image analysis. Depicted in (a) is the results of the image analysis performed on the Flat Constant geometry, compared with the scaled up input data. In (b), the same is shown for the Flat Linear Geometry. The general trends of the expected output are reflected in the measurements of both beam thickness and cell spacing. The behaviour going from linear to curved input data is as expected. There are clear deviations of the measurements to the expected curves however. The cell spacings start and end approximately as expected, but overestimate the values in between, at most around the middle of the radius. Both beam thicknesses closely reproduce the expected output starting from a radius of around $20\,\%$, but before this, there is a large deviation of a similar shape to the initial region of the average measurements from the biological specimens. There is also a small deviation close to the end that differs between the two geometries.

to drastically change both their size and material properties in under 30 min after being taken out of their controlled environment. That they seem to loose their moisture so quickly, when exposed to ambient conditions, makes it unlikely that the cocoon is sufficient at protecting from desiccation, as soon as the humidity of the environment sinks to levels of around 50 %. The drastic shift does elude to the structure having held a lot of moisture initially, however. It is possible that the terrestrial leeches have developed a mechanism to make their cocoons highly adaptive to environmental conditions, though they may also not be intended to ever be subjected to a lower humidity. Petersen et al. (2008) showed resistance of the cocoons of the earthworm *Dendrobaena octaedra* to slow desiccation and eluded to such conditions arising with some frequency in the upper layers of the soil. However, earthworm cocoons heavily differ from the cocoons of the investigated leech and do not have the complex wall structures that were observed here (Chaudhuri and Datta, 2020). In situ studies on *Hirudo sp.* that explore the conditions that the cocoons experience, as well as an investigation of the interactions of their wall structure and material with moisture could lead to new discoveries and explain the phenomenon that occurred during preparation.

The results gathered by the analysis of dry cocoons affirmed the observations of Saidel et al. (2018), showing a complex cellular structure in the form of a network of thin beams, whose thickness decreased from the inner to the outer radius. On top of this, a gradient of the cell spacing was discovered (s. Figure 9). Although the methodology showed some errors in its validation that will have affected the measured results, they were small compared to the gradients measured in some sections (s. Figure 16). All beam thickness measurements after a radius of 20 % seem to be nearly perfectly reliable, in fact. The two local maxima of the beam thickness at lower radii found in Figure 9 however, may not be a result of real measurements, but the products of the errors found in Figure 16 in the same general area. This discrepancy can most likely be explained by the effect of having the inner wall of solid material at the most inner radii. The local thickness implementation of PoreSpy used to measure beam thicknesses tries to project a sphere outwards from a point of one material, until it hits another material (Gostick et al., 2019). If the geometry is that of a solid wall, there is less surface that the sphere could hit compared to thin beams, meaning that the measurements will on average be higher, even if the thickness of the wall may be equal to that of the beam. The smaller errors at the outer radii are likely caused by the algorithm artificially restricting the outer bounds of the lattice and disrupting its natural continuation. Effects of the boundary restrictions imposed by the algorithm are probably also what caused the curvature of the optimally straight cell spacing data. Because there are only up to five rows of cells in the thin wall produced by the algorithm, these effects may have impacted the entire curve, instead of just the outer parts, like for the beam thickness.
There was practically no discrepancy found for the relative noise of the biological measurements and the measurements of a geometry created by the algorithm, meaning this aspect could be fully reproduced.
In general the relative accuracy can be deemed sufficient for the scope of this thesis. It is most likely possible to produce an image analysis method that can eliminate nearly all errors and also provide absolute precision, meaning it may be able to directly measure the quantity, not

just proportional values. It is possible that a study that improves on the current image analysis methodology would have to create custom implementations of the functions that were provided by packages like PoreSpy to adapt to the specific challenges presented by the analysis of thin, curved walls with cellular structures.

The FEA showed RBL that were up to 3.38 times higher compared to compression tests with very similar conditions. This showcases that the methodology used is completely unsuitable to predict the RBL quantitatively in a structural context. No part that is intended to be used in a real structural application should be evaluated based on the RBL it may withstand according to the setup, especially since it overestimated the capabilities of the two simulated models. This is most likely caused by the interaction of the tie knot constraint to the implement that was displaced directly. The nodes of the tie constraints, where forces are supposed to be transmitted in the y-direction, instead showed reaction forces near zero. This also explains the upper compressed region of no stress of the Curved Shell geometry (s. Figure 11b). The expectation was that these reaction forces would directly matchthose found in the two constraints on the bottom. This would be the observed behaviour both practically and analytically. But the absence of higher reaction forces in this area suggests that they had to have been absorbed somewhere else to produce the deformation of the geometry, causing them to somehow be transferred to the bottom constraints. This would certainly not be intended and most likely caused by a user error, utilizing tools that were not meant to be used in conjunction with one another. Park et al. (2018) showed that linear static and contact analyses can be accurately solved with CalculiX, the solver used by PrePoMax. If instead of direct displacement of a compression implement attached by tie constraints, a contact analysis was performed, the results would most likely be far more accurate. Another factor that might have lead to further inaccuracies is that the material properties might not have been fully correct. In material tests the specimens proved exceedingly flexible (s. Figure 13). Even after having their curvature straightened out, they showed little signs of permanent damage. The Curved Shell specimens even returned to their original state completely after the compression. This eludes to the PLA having additives that reduce stiffness, but increase flexibility. A direct evaluation of the material properties of the PLA may lead to further improvement of the FEA. Despite the low accuracy of the simulated RBL quantitatively, qualitatively the results matched those of the compression tests and are therefore deemed sufficient to verify the hypotheses that are purely comparative in nature (s. Figure 14). It has to be added however that the practical compression tests lead to invaluable insights and made the shortcomings of the FEA apparent. This underlines that FEA can never be a replacement for practical testing and should always be used in conjunction with it.

Both the measurements and material tests showed a much higher RBL for curved structures generated from the cocoon-inspired algorithm when compared to the simple uniform shell (s. Table 8 and 9). In compression tests, the bio-inspired Curved Cocoon Comparison geometry had a 3.55 times RBL than the higher mass the Curved Shell. This means that Hypothesis 1 must be rejected.
Though it has to be said that there was no clear plateau indicating where radial buckling starts at the displacement of 5.3 mm for the Curved Shell, as there was for the Curved Cocoon Com-

parison in material tests. This means that the extraction of the RBL at this exact displacement may not be completely accurate. The compression curves extending beyond a displacement of 5.3 mm are depicted in Figure 17.

Even if no clear RBL can be determined here, it is apparent that the solid wall of the uni-

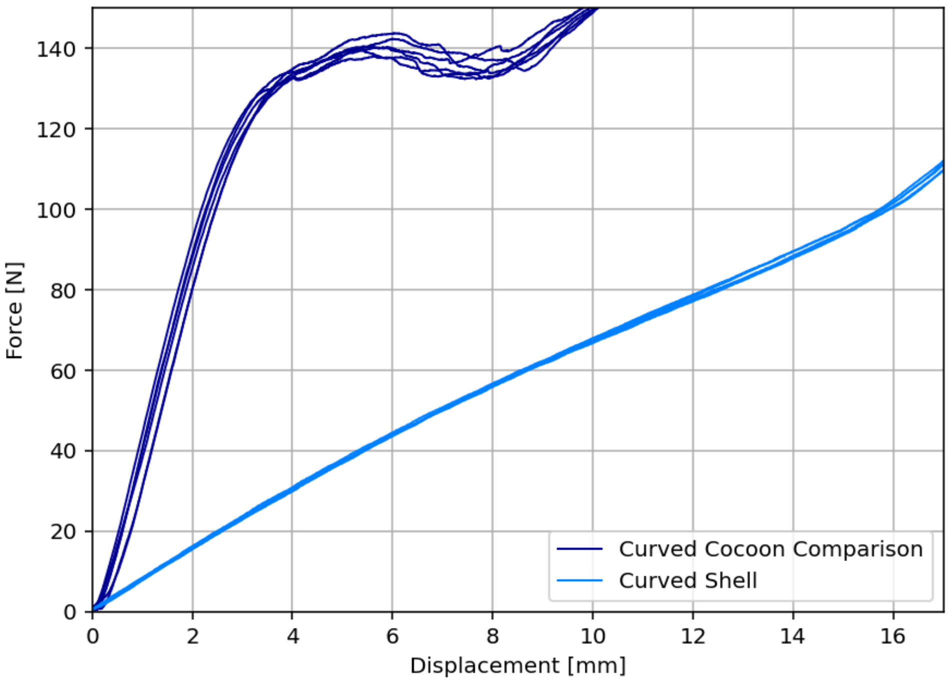

Figure 17: Comparison of the extended curves of all compression tests. Both the curves of the Curved Cocoon Comparison and the Curved Shell are shown fully, up to the point, where their geometrical curvature is fully straightened out and only the wall material is compressed. The Curved Cocoon Comparison shows a far more aggressive load response to the displacement and shows a clear plateau, which was determined to correspond to radial buckling. It shows the higher loads at all displacements. At a displacement of 5.3 mm, the reaction forces of the specimens no longer increased, which is why it was determined as the displacement at which the RBL of occurs. This RBL was measured at 139.7 N. At a displacement of around 8 mm, the curve increased exponentially, as the wall is compressed directly. This occurs much earlier, because the thickness of the geometry is much higher. The Curved Shell measurements show a much slower increase of forces, but also no clear plateau, so a clear displacement at which radial buckling occurs is not discernible. At a displacement of 16 mm, where a force of 101.4 N was measured, the force starts to rise exponentially, meaning that the wall material was starting to get compressed directly.

form shell provides far less resistance to the load compared to the bio-inspired structure. This response makes it highly likely that the cocoon, that it is closely based on, is mechanically optimized to withstand such loads. To outright confirm this assertion, leech cocoons would have to be examined in compression tests themselves, as the abstraction of the cellular wall structures into the algorithm may have introduced optimizations that are not present in the bio-inspiration itself.

Under the assumption that the results of the FEA are qualitatively accurate, the edged geometry that was created from the cocoon-inspired algorithm was also above the one generated with a uniform shell operation, although to a smaller extent than for the curved geometries. This means that Hypothesis 2 must also be discarded.

Despite this, the simulation has shown that there is a unique mode of failure for the cocoon-inspired edged geometry when compared to the curved geometry. When load is applied at the

edge, like was the case in the FEA, there are only a few thin beams locally that have to bear the entire compressive load. This leads to those beams buckling locally, before the two sides of the geometries are bent laterally (s. Figure 12).
Such occurrences illuminate how the cocoon wall structure of *Hirudo sp.* may not be optimal for geometry that have edges, especially when the edges may directly be subjected to loads. The behaviour of similar structures when applied to edged geometry that is compressed on flat sides will likely produce different modes of failure.

Now that it is clear that the cocoon-inspired algorithm presents an optimization for an increased radial buckling load that may be used for lightweighting, it is of particular interest how that optimization compares to existing lightweighting techniques for different load cases. The natural points of comparison would be the periodical cells, such as honeycomb- or truss structures, that are in use for lightweight applications in metal foams, because of their high stiffness to weight ratio (Sanders, 2004).
The comparatively high performance of the Curved Cocoon Comparison geometry, despite it having the lowest mass, is also a particularly interesting observation. This geometry's only difference compared to some others was the gradients provided to the algorithm for its creation. Such observations make it apparent that an optimization of these parameters can lead to higher performance at lower masses. Since the entire algorithm is native to nTop, which specializes in optimizations for lattices, such as the Voronoi structure employed here, an implementation could be accomplished easily. This process may produce highly performant cocoon-inspired lightweight structures specifically designed for any given application.

5 Conclusion

The wall structure of both dry and fresh cocoons of *Hirudo sp.* were examined with a Micro-CT-Scanner. Then, image analysis was conducted on the scans to examine the radial gradients of the cellular structure present there. With the insights and data gathered this way, a light weighting algorithm was created. Curved and Edged geometries created by the algorithm were examined along comparable uniform shells in regards to buckling under radial compression. Both compression tests and FEA were conducted for this purpose. The employed methodology was also examined for relative accuracy.

Despite the current understanding of the cocoon's complex cellular structures serving as protection from desiccation, the results showed that geometries similar to it provided greater resistance to radial buckling than unoptimized shells. This hints at the cocoon of *Hirudo sp.* providing mechanical protection as well. Fresh cocoons also quickly reacted with ambient humidity and changed their size and properties, which may be an intentional mechanism to adapt to different environments.

The results illuminate that the cocoons of these animals are yet poorly understood and studying them may be the source of several novel discoveries. Some of the observations made here could represent new avenues for further investigations of both the cocoons of *Hirudo sp.* and biomimetic lightweight structures inspired by it. Further gradient optimization of the algorithm introduced here may have the potential to elevate this novel lightweighting approach to provide advantages in certain aspects compared to the lightweight structures that are in use currently.

6 Sources

6.1 Literature

Chaudhuri, P. S. and Datta, R. (2020). Studies on Cocoons of Three Epigeic Earthworm Species *Perionyx excavatus* (Perrier), *Perionyx ceylanensis* (Michaelsen) and *Eudrilus eugeniae* (Kinberg) with SEM Observations. *Proceedings of the Zoological Society*, 73(4):430–440.

Craven, P. and Wahba, G. (1978). Smoothing noisy data with spline functions: Estimating the correct degree of smoothing by the method of generalized cross-validation. *Numerische Mathematik*, 31(4):377–403.

Efstathiadis, A., Symeonidou, I., Tsongas, K., Tzimtzimis, E. K., and Tzetzis, D. (2023). 3D Printed Voronoi Structures Inspired by Paracentrotus lividus Shells. *Designs*, 7(5):113.

Farah, S., Anderson, D. G., and Langer, R. (2016). Physical and mechanical properties of PLA, and their functions in widespread applications — A comprehensive review. *Advanced Drug Delivery Reviews*, 107:367–392.

Feng, F., Xiong, S., Liu, Z., Xian, Z., Zhou, Y., Kobayashi, H., Kawamoto, A., Nomura, T., and Zhu, B. (2023). Cellular topology optimization on differentiable Voronoi diagrams. *International Journal for Numerical Methods in Engineering*, 124(1):282–304.

Gostick, J., Khan, Z., Tranter, T., Kok, M., Agnaou, M., Sadeghi, M., and Jervis, R. (2019). PoreSpy: A Python Toolkit for Quantitative Analysis of Porous Media Images. *Journal of Open Source Software*, 4(37):1296.

Groen, J. P., Thomsen, C. R., and Sigmund, O. (2021). Multi-scale topology optimization for stiffness and de-homogenization using implicit geometry modeling. *Structural and Multidisciplinary Optimization*, 63(6):2919–2934.

Harris, C. R., Millman, K. J., Van Der Walt, S. J., Gommers, R., Virtanen, P., Cournapeau, D., Wieser, E., Taylor, J., Berg, S., Smith, N. J., Kern, R., Picus, M., Hoyer, S., Van Kerkwijk, M. H., Brett, M., Haldane, A., Del Río, J. F., Wiebe, M., Peterson, P., Gérard-Marchant, P., Sheppard, K., Reddy, T., Weckesser, W., Abbasi, H., Gohlke, C., and Oliphant, T. E. (2020). Array programming with NumPy. *Nature*, 585(7825):357–362.

Hu, Z., Thiyagarajan, K., Bhusal, A., Letcher, T., Fan, Q. H., Liu, Q., and Salem, D. (2017). Design of ultra-lightweight and high-strength cellular structural composites inspired by biomimetics. *Composites Part B: Engineering*, 121:108–121.

Hübner, D., Herrnböck, L., Wein, F., Mergheim, J., Steinmann, P., and Stingl, M. (2023). Buckling optimization of additively manufactured cellular structures using numerical homogenization based on beam models. *Archive of Applied Mechanics*, 93(12):4445–4465.

Li, Q., Hong, Q., Qi, Q., Ma, X., Han, X., and Tian, J. (2018). Towards additive manufacturing oriented geometric modeling using implicit functions. *Visual Computing for Industry, Biomedicine, and Art*, 1(1):9.

Li, Y., Li, J., Sun, X., Jing, Y., and Eerhemubayaer (2011). Analysis of winding stability of short-circuit test model for extra-high voltage power transformer. In *2011 International Conference on Electrical Machines and Systems*, pages 1–4, Beijing, China. IEEE.

Maiti, A., Small, W., Lewicki, J. P., Weisgraber, T. H., Duoss, E. B., Chinn, S. C., Pearson, M. A., Spadaccini, C. M., Maxwell, R. S., and Wilson, T. S. (2016). 3D printed cellular solid outperforms traditional stochastic foam in long-term mechanical response. *Scientific Reports*, 6(1):24871.

Maitland, P. S., Phillips, D. S., and Gaywood, M. J. (2000). Notes on distinguishing the cocoons and the juveniles of *Hirudo medicinalis* and *Haemopis sanguisuga* (Hirudinea). *Journal of Natural History*, 34(5):685–692.

Ou, Q., Luo, L., Li, Y., Han, R., and Peng, Y. (2023). An Improved Radial Buckling Analysis Method and Test Investigation for Power Transformer Under Short Circuit Impact. *IEEE Transactions on Power Delivery*, 38(4):2854–2863.

Park, S.-K., Seo, D.-W., Jeong, H., and Kim, M. (2018). Performance Evaluation of Open-Source Structural Analysis Solver, CalculiX and Code-Aster, for Linear Static and Contact Problems. *ICIC Express Letters*, 12(7):655–662.

Petersen, C. R., Holmstrup, M., Malmendal, A., Bayley, M., and Overgaard, J. (2008). Slow desiccation improves dehydration tolerance and accumulation of compatible osmolytes in earthworm cocoons (*Dendrobaena octaedra* Savigny). *Journal of Experimental Biology*, 211(12):1903–1910.

Phillips, A. J., Govedich, F. R., and Moser, W. E. (2020). Leeches in the extreme: Morphological, physiological, and behavioral adaptations to inhospitable habitats. *International Journal for Parasitology: Parasites and Wildlife*, 12:318–325.

Saidel, W. M., Saglam, N., Salas-de La Cruz, D., Saunders, R., and Shain, D. H. (2018). Elaborate ultrastructure of the *Hirudo* (Annelida: Hirudinae) cocoon surface. *Journal of Morphology*, 279(4):545–553.

Sanders, W. S. (2004). Lightweight Cellular Metals with High Structural Efficiency. In Senkov, O. N., Miracle, D. B., and Firstov, S. A., editors, *Metallic Materials with High Structural Efficiency*, volume 146, pages 419–424. Kluwer Academic Publishers, Dordrecht. Series Title: NATO Science Series II: Mathematics, Physics and Chemistry.

Schliecker, G. (2002). Structure and dynamics of cellular systems. *Advances in Physics*, 51(5):1319–1378.

Virtanen, P., Gommers, R., Oliphant, T. E., Haberland, M., Reddy, T., Cournapeau, D., Burovski, E., Peterson, P., Weckesser, W., Bright, J., Van Der Walt, S. J., Brett, M., Wilson, J., Millman, K. J., Mayorov, N., Nelson, A. R. J., Jones, E., Kern, R., Larson, E., Carey, C. J., Polat, , Feng, Y., Moore, E. W., VanderPlas, J., Laxalde, D., Perktold, J., Cimrman, R., Henriksen, I., Quintero, E. A., Harris, C. R., Archibald, A. M., Ribeiro, A. H., Pedregosa, F., Van Mulbregt, P., SciPy 1.0 Contributors, Vijaykumar, A., Bardelli, A. P., Rothberg, A., Hilboll, A., Kloeckner, A., Scopatz, A., Lee, A., Rokem, A., Woods, C. N., Fulton, C., Masson, C., Häggström, C., Fitzgerald, C., Nicholson, D. A., Hagen, D. R., Pasechnik, D. V., Olivetti, E., Martin, E., Wieser, E., Silva, F., Lenders, F., Wilhelm, F., Young, G., Price, G. A., Ingold, G.-L., Allen, G. E., Lee, G. R., Audren, H., Probst, I., Dietrich, J. P., Silterra, J., Webber, J. T., Slavič, J., Nothman, J., Buchner, J., Kulick, J., Schönberger, J. L., De Miranda Cardoso, J. V., Reimer, J., Harrington, J., Rodríguez, J. L. C., Nunez-Iglesias, J., Kuczynski, J., Tritz, K., Thoma, M., Newville, M., Kümmerer, M., Bolingbroke, M., Tartre, M., Pak, M., Smith, N. J., Nowaczyk, N., Shebanov, N., Pavlyk, O., Brodtkorb, P. A., Lee, P., McGibbon, R. T., Feldbauer, R., Lewis, S., Tygier, S., Sievert, S., Vigna, S., Peterson, S., More, S., Pudlik, T., Oshima, T., Pingel, T. J., Robitaille, T. P., Spura, T., Jones, T. R., Cera, T., Leslie, T., Zito, T., Krauss, T., Upadhyay, U., Halchenko, Y. O., and Vázquez-Baeza, Y. (2020). SciPy 1.0: fundamental algorithms for scientific computing in Python. *Nature Methods*, 17(3):261–272.

Widiyanto, I., Prabowo, A., Muttaqie, T., Muhayat, N., Yaningsih, I., Tjahjana, D., Juwana, W., and Miyazaki, T. (2022). Effects of geometry and material factors on the behavior of stiffened offshore pipe structures under hydrostatic pressure. *Journal of Applied Engineering Science*, 20(4):1103–1121.

Yang, Y., Song, X., Li, X., Chen, Z., Zhou, C., Zhou, Q., and Chen, Y. (2018). Recent Progress in Biomimetic Additive Manufacturing Technology: From Materials to Functional Structures. *Advanced Materials*, 30(36):1706539.

Yuan, Y., Zhang, Y., Ruan, D., Zhang, A., Liang, Y., Tan, P., and Chen, P. (2023). Deformation and failure of additively manufactured Voronoi foams under dynamic compressive loadings. *Engineering Structures*, 284:115954.

6.2 Other Sources

Bambu Lab (n. d.). Bambu Filament Technical Data Sheet V3.0. `https://store.bblcdn.com/s7/default/23b4cf2b83d5470bb96d19970b5f3ae8/Bambu_ABS_Technical_Data_Sheet_V3.pdf`. Accessed on November 12, 2025.

Verein Deutscher Ingenieure (2012). Biomimetics — Conceptions and Strategy, Differences Between Biomimetic and Conventional Methods/Products. VDI-Standard 6220, DIN Media, Berlin.

Erklärung über das eigenständige Erstellen der Arbeit

Hiermit versichere ich, dass ich die vorliegende Arbeit selbstständig verfasst und keine anderen als die angegebenen Quellen und Hilfsmittel benutzt habe. Die Stellen der Arbeit, die anderen Werken dem Wortlaut oder dem Sinn nach entnommen wurden, sind durch Angaben der Herkunft kenntlich gemacht. Diese Erklärung erstreckt sich auch auf die in der Arbeit enthaltenen Grafiken, Skizzen sowie bildlichen Darstellungen. Die Arbeit habe ich in gleicher oder ähnlicher Form auch auszugsweise noch nicht als Bestandteil einer Prüfungs- oder Studienleistung vorgelegt. Ich versichere, dass die eingereichte elektronische Version der Arbeit vollständig mit der Druckversion übereinstimmt und stimme einer elektronischen Überprüfung der Arbeit mittels Plagiatssoftware zu.

Ich versichere, dass ich keine KI-basierten Tools verwendet habe, deren Nutzung mit der prüfenden Person nicht schriftlich verabredet wurde. Ich bin mir bewusst, dass die Verwendung von Texten oder anderen Inhalten und Produkten, die durch KI-basierte Tools generiert wurden, keine Garantie für deren Qualität darstellt. Ich übernehme die Verantwortung für die abgegebene Arbeit und die darin enthaltenen Inhalte. Ich versichere zudem, dass in der vorliegenden Arbeit mein gestalterischer Einfluss überwiegt. Sämtliche wörtlichen oder sinngemäßen Übernahmen und Zitate, sowie alle Abschnitte, die mithilfe von KI-basierten Tools entworfen, verfasst und/oder bearbeitet wurden, sind von mir kenntlich gemacht und nachgewiesen. Die Form der Kennzeichnung wird zwischen der prüfenden Person und Prüfling abgestimmt.

Mir ist bekannt, dass ein Verstoß gegen die genannten Punkte prüfungsrechtliche Konsequenzen haben und insbesondere dazu führen kann, dass die Prüfungsleistung mit „nicht ausreichend“ bzw. die Studienleistung mit „nicht bestanden“ bewertet wird und bei mehrfachem oder schwerwiegendem Täuschungsversuch eine Exmatrikulation erfolgen kann.

Bremen, am 11.12.2025 Tino Marte